

REVIEW

## A hybrid approach to multi-scale modelling of cancer

BY J. M. OSBORNE<sup>1,2,\*†</sup>, A. WALTER<sup>3,†</sup>, S. K. KERSHAW<sup>1</sup>, G. R. MIRAMS<sup>4</sup>,  
A. G. FLETCHER<sup>2,5</sup>, P. PATHMANATHAN<sup>1</sup>, D. GAVAGHAN<sup>1,2</sup>, O. E. JENSEN<sup>6</sup>,  
P. K. MAINI<sup>2,5</sup> AND H. M. BYRNE<sup>6</sup>

<sup>1</sup> Oxford University Computing Laboratory, Wolfson Building, Parks Road,  
Oxford OX1 3QD, UK

<sup>2</sup> Oxford Centre for Integrative Systems Biology, Department of Biochemistry,  
South Parks Road, Oxford OX1 3QU, UK

<sup>3</sup> Oxford Centre for Collaborative Applied Mathematics, and <sup>5</sup> Centre for  
Mathematical Biology, Mathematical Institute, 24–29 St Giles',  
Oxford OX1 3LB, UK

<sup>4</sup> Department of Physiology, Anatomy and Genetics, Parks Road,  
Oxford OX1 3PT, UK

<sup>6</sup> Centre for Mathematical Medicine and Biology, School of Mathematical  
Sciences, University of Nottingham, University Park,  
Nottingham NG7 2RD, UK

In this paper, we review multi-scale models of solid tumour growth and discuss a middle-out framework that tracks individual cells. By focusing on the cellular dynamics of a healthy colorectal crypt and its invasion by mutant, cancerous cells, we compare a cell-centre, a cell-vertex and a continuum model of cell proliferation and movement. All models reproduce the basic features of a healthy crypt: cells proliferate near the crypt base, they migrate upwards and are sloughed off near the top. The models are used to establish conditions under which mutant cells are able to colonize the crypt either by top-down or by bottom-up invasion. While the continuum model is quicker and easier to implement, it can be difficult to relate system parameters to measurable biophysical quantities. Conversely, the greater detail inherent in the multi-scale models means that experimentally derived parameters can be incorporated and, therefore, these models offer greater scope for understanding normal and diseased crypts, for testing and identifying new therapeutic targets and for predicting their impacts.

**Keywords:** cancer; multi-scale model; cell-centre model; cell-vertex model; continuum model;  
colorectal cancer

\*Author for correspondence (james.osborne@comlab.ox.ac.uk).

†These authors contributed equally to the study.

Electronic supplementary material is available at <http://dx.doi.org/10.1098/rsta.2010.0173> or via <http://rsta.royalsocietypublishing.org>.

One contribution of 12 to a Theme Issue ‘Theory of hybrid dynamical systems and its applications to biological and medical systems’.

## 1. Introduction

Population expansion and ageing mean that the number of lives claimed annually by cancer will increase further unless more effective measures for its prevention and treatment are found (Jemal *et al.* 2009). Increased understanding of the processes that drive cancer progression is fundamental to achieving these goals. Cancer develops when genetic and epigenetic changes disrupt the processes that maintain cellular homeostasis by regulating cell division, growth, movement and apoptosis. Successful angiogenesis, the formation of new blood vessels, is also necessary for tumours to progress to the rapid phase of vascular growth. To confound matters, these coupled processes act over a spectrum of spatial and temporal scales. The spatial scales range from the subcellular to the cellular and macroscopic levels, while the timescales vary from seconds (or less) for signal transduction to months (and years) for tumour-doubling times. Traditionally, partial differential equation models have been used to simulate the growth of solid tumours and other biological tissues. However, they are not well suited to study multi-scale systems and are not valid for small numbers of cells. This is important when modelling cancer, as a mutation initially creates a single abnormal cell. Since it is now possible to image individual cells, this is a natural level at which to focus when developing models that can be validated. However, numerous questions are raised, including ‘which cell-based description should we use?’, ‘what level of detail should be included at each scale?’ and ‘as cell numbers increase, how do we move from the discrete system to the continuum?’ Multi-scale models provide a natural framework for addressing such questions (Zheng *et al.* 2005).

Correspondingly, the approaches used to model avascular tumours have become increasingly varied and complex. There are now several multi-scale representations of cellular and tissue processes in avascular tumours (see Martins *et al.* 2007; Preziosi & Tosin 2009, for reviews). Spheroidal avascular tumours grow up to 1 mm in diameter, their size being limited by the diffusion of oxygen and other nutrients to the centre of the tumour.

In order to grow larger, a tumour must stimulate the inward growth of new blood vessels to supply it with the nutrients it needs to survive. This process, and the consequent development of a vascular tumour, has become an increasingly large field of study in recent years. Multi-scale models range from simple ones in which cellular automata are coupled with reaction–diffusion equations for oxygen and glucose that act on a macroscale (Patel *et al.* 2001; Smallbone *et al.* 2007), through to more complex models that incorporate blood flow, vascular remodelling (McDougall *et al.* 2002; Owen *et al.* 2009) and details of subcellular processes such as the cell cycle and protein expression (Alarcón *et al.* 2003; Shirinifard *et al.* 2009). Such models enable us to investigate the effect of feedback between subcellular, cellular and tissue processes on the morphology and composition of vascular tumours and their response to chemotherapy (Byrne *et al.* 2006). The frameworks for running simulations of such models are large and complex. As a result, several collaborative software projects such as CompuCell3D (Merks & Glazier 2005) and Chaste (Cancer, heart and soft-tissue environment; Pitt-Francis *et al.* 2009) have been developed to tackle such problems. In this paper, we describe some of the multi-scale approaches that have been used to model early colorectal cancer (CRC) in

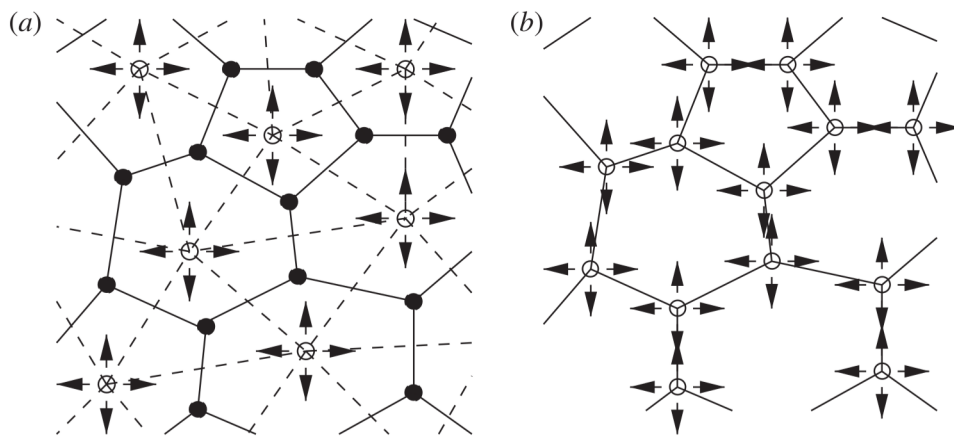


Figure 1. Schematic representations of the cell-level models. (a) Cell-centre model: the size and shape of the cells (bounded by solid lines and filled circles) are determined from a Voronoi tessellation of the cell centres (open circles). (b) Cell-vertex model: cell size and shape are defined by the positions of vertices at cell junctions (open circles). Evolution of the epithelium arises through motion of centres or vertices, as indicated by arrows.

Chaste, comparing in particular cell-centre and cell-vertex models with a continuum description of epithelial dynamics in a colorectal crypt. We assess the relative merits of each model and discuss their suitability for studying the colorectal crypt.

## 2. Multi-scale and continuum model frameworks

The intestine consists of a series of regularly spaced, test-tube-shaped crypts, covered with a protective layer of epithelial cells. CRC, the second most common malignancy in Europe (Ferlay *et al.* 2007), typically originates from the epithelium, as a result of genetic and epigenetic changes. Renewal of the intestinal epithelium occurs every few days and requires coordination of cell proliferation, migration, differentiation and apoptosis. Stem cells at the base of each crypt proliferate to produce transit cells, which divide several times before differentiating into the functioning cells of the gut. The new cells drive the upward movement of existing cells, which undergo apoptosis (cell death) and are shed into the lumen when they reach the top of a crypt. Crypt homeostasis is maintained by position-dependent extracellular signals (e.g. basement membrane composition, Wnt levels) and intracellular gene levels (Gaspar & Fodde 2004). Mutations in the associated regulatory networks disrupt homeostasis, leading to increased cell proliferation, crypt deformation and fission and polyp formation (Preston *et al.* 2003).

The above description highlights the multi-scale nature of the dynamics of normal and diseased crypt epithelia. In §3, we introduce the general, ‘middle-out’ multiscale framework that we have developed to simulate the dynamics of a colorectal crypt (Pitt-Francis *et al.* 2009; van Leeuwen *et al.* 2009) and present two alternative cell-based models that can be incorporated into the framework: a cell-centre model and a cell-vertex model (figure 1).

(a) *Multi-scale model framework*

The multi-scale model that we use couples processes acting at the tissue, cellular and subcellular scales. To facilitate comparison of the cell-based models, common subcellular and tissue-level models are used to describe cell proliferation.

(i) *Tissue- and subcellular-level models*

The crypt is viewed as a two-dimensional cylindrical surface of height  $H_C = 20$  cell diameters and circumference  $W_C = 10$  cell diameters, where we estimate that a cell diameter is approximately 8 µm (Drasdo & Loeffler 2001). The independent variables  $x \in (0, W_C)$  and  $y \in (0, H_C)$  represent, respectively, circumferential distance and distance from the crypt base. Periodic boundary conditions are imposed on  $x = 0$  and  $x = W_C$ , and no cells are removed through the crypt base ( $y = 0$ ). Cells are removed, or sloughed off, when they reach the lumen ( $y = H_C$ ).

We suppose that the crypt contains healthy and mutant cells and that there is a spatial gradient in Wnt along the crypt axis, so that Wnt levels are high near  $y = 0$  and low near  $y = H_C$ . Owing to its small size, we assume a nutrient-rich environment and do not include a vasculature in the model. Mutant and normal cells are assumed to differ in their rates of cell proliferation and their cell-cell and cell-substrate adhesion properties (Sansom *et al.* 2004; Bienz 2005). Specifically, healthy cells proliferate in the bottom third of the crypt ( $0 \leq y \leq H_W = H_C/3$ ) where Wnt levels exceed a threshold level, whereas mutant cells proliferate throughout the crypt, irrespective of the local Wnt concentration. The mutant cells also exhibit increased stromal adhesion and stronger cell-cell adhesion.

The cell cycle of both normal and mutant cells is assumed to vary stochastically, with the total duration of the G<sub>1</sub>, S, G<sub>2</sub> and M phases being sampled from a normal distribution, with mean 16 h and s.d. 1 h.

(ii) *Cell-centre model*

We extend a lattice-free, cell-centre model (figure 1*a*) developed by Meineke *et al.* (2001), and described by van Leeuwen *et al.* (2009). Each cell is treated as a discrete entity and adjacent cell centres are connected by linear springs. Neighbouring cells are determined by a Delaunay triangulation while cell shapes are determined by a Voronoi tessellation. The equations of motion are developed by neglecting inertial effects and balancing viscous drag on cell centres with cell-cell interaction forces associated with the compression and extension of the springs. The equations of motion are

$$\mu_i \frac{d\mathbf{r}_i}{dt} = \sum_{j \in S_i} k_{ij}(|\mathbf{r}_i - \mathbf{r}_j| - s_{ij}(t)) \frac{(\mathbf{r}_j - \mathbf{r}_i)}{|\mathbf{r}_j - \mathbf{r}_i|}, \quad i = 1, \dots, n, \quad (2.1)$$

where  $\mathbf{r}_i$  is the position of cell centre  $i$ ,  $n$  is the total number of cells,  $s_{ij}(t)$  and  $k_{ij}$  are the natural length and strength, respectively, of the spring connecting cell centres  $i$  and  $j$ ,  $S_i$  is the set of cells that are adjacent to cell  $i$ ,  $\mu_i$  is the drag coefficient, which depends on cell  $i$ 's type, and  $t$  is time. The drag term models cell-stroma adhesion.

When cell  $i$  divides, its daughter cell  $j$  is placed a distance 0.1 cell diameters from cell  $i$ , in a randomly chosen direction. To model cell growth during M phase, the rest length of the spring connecting parent and daughter cell,  $s_{ij}(t)$ , increases from 0.1 to 1 during the last hour of the cell cycle;  $s_{ij}(t) = 1$  for all other connections.

### (iii) Cell-vertex model

In the cell-vertex model (figure 1*b*), the size and shape of each cell is dictated by the movement of its vertices. We introduce a free energy  $U$ , with contributions from each cell, whose gradient with respect to vertex displacement exerts a force on each cell vertex which, if inertial effects are neglected, is balanced by a drag force proportional to the vertex velocity. We decompose  $U$  for cell  $j$  into a deformation energy,  $U_D^j$ , a membrane surface tension energy,  $U_S^j$ , and a cell-cell adhesion energy,  $U_A^j$  (Nagai & Honda 2001). The deformation term ensures that cells attain their target area (cell height is assumed constant). Membrane surface tension is included to conserve membrane length and acts to drive cells to a circular shape. The cell-cell adhesion energy term represents the free energy associated with cadherin and other bonds on the membrane; it is proportional to the contact area between two cells and depends on their types. The equations of motion are as follows:

$$\eta_i \frac{d\mathbf{r}_i}{dt} = -\nabla_i \sum_{j=1}^n (U_D^j + U_S^j + U_A^j), \quad (2.2)$$

$$= -\nabla_i \sum_{j=1}^n \left( \lambda(A_j - A_{T,j})^2 + \beta(C_k - C_{T,j})^2 + \sum_{m=1}^{M_j} \gamma_S L_{j,m} \right), \quad (2.3)$$

where  $\mathbf{r}_i$  is the position of vertex  $i$ ,  $\eta_i$  is the associated drag (averaged over values assigned to all cells containing the vertex),  $\nabla_i$  is the gradient with respect to  $\mathbf{r}_i$  and  $n$  denotes the number of cells in the system. In equation (2.3),  $A_j$  is the cross-sectional area of cell  $j$ ,  $C_j$  is the perimeter (in two dimensions) and  $M_j$  is the number of vertices of cell  $j$ .  $L_{j,m}$  is the length of the line connecting vertices  $m$  and  $m+1$ . Similarly,  $A_{T,j}$  is the cell's natural (or target) area, and  $C_{T,j} = 2(\pi A_{T,j})^{1/2}$  its natural perimeter. Finally  $\lambda$  and  $\beta$  are positive constants, and  $\gamma_S$  is a positive constant whose value depends on whether edge  $m$  is on an external boundary or not (Honda *et al.* 1984; Nagai & Honda 2001).

On completing its cell cycle, a cell splits into two equal parts, along its short axis (Sausedo *et al.* 1997). The target areas of both daughter cells are set to  $A_T = \pi/8$  [cell diameter] $^2$  and increase linearly during the first hour of their cell cycles towards  $A_T = \pi/4$  [cell diameter] $^2$ , the target area of a mature cell.

### (iv) Implementation of multi-scale models

The cell-centre and cell-vertex models are implemented in the Chaste framework (Pitt-Francis *et al.* 2009), which has been released under the LGPL 2.1 open source licence and is available at <http://www.comlab.ox.ac.uk/chaste>. The parameter values are given in the electronic supplementary material. The crypt size is taken from Meineke *et al.* (2001) and the cell-cycle times from

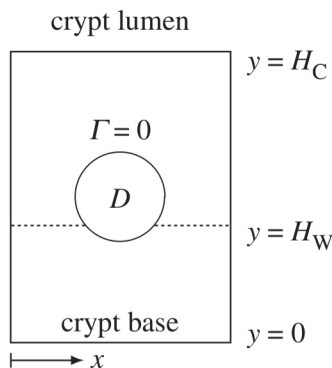


Figure 2. Schematic representation of the crypt in the continuum model. Mutant cells occupy the domain  $D$  while normal cells surround it.

Sunter *et al.* (1979). The parameters for the cell-vertex model were chosen to ensure that the crypt was in a quasi-steady state (the net rate of cell proliferation balancing the rate cells are removed from the top of the crypt) and the vertex movement was stable (they moved smoothly and did not pass through edges of other cells). The parameters for the cell-centre model were chosen by matching the velocity of the cells with that for the cell-vertex model. For the system described above, it takes about 25 min (130 min) to simulate 1000 cell-hours on a desktop PC (2.4 GHz processor) using the cell-centre (cell-vertex) model. Details of numerical parameters used can be found in van Leeuwen *et al.* (2009).

### (b) Continuum model

For comparison with the two cell-based models, we also develop a continuum model for the proliferation and movement of cells within the crypt. It is assumed that there are no gaps in the epithelium, the cell density is constant and two distinct cell populations, separated by a closed, moving interface  $\Gamma(x, y, t) = 0$  (figure 2), are considered: normal (N) and mutant (M) cells. Mutant cells occupy the domain  $D$  bounded by  $\Gamma = 0$ . The epithelium is characterized by an average velocity field  $\mathbf{v}(x, y, t)$  and pressure field  $p(x, y, t)$ . To mimic Wnt dependence, normal cells lying outside  $D$  proliferate in the region  $0 < y \leq H_W$  at rate  $k^-$  while mutant cells in  $D$  proliferate uniformly at rate  $k^+$ , so that  $\nabla \cdot \mathbf{v} = k^\pm$ . Following Greenspan (1976), Darcy's law is used to model cell motion, so that  $\mu^\pm \mathbf{v} = -\nabla p$ , where  $\mu^-$  ( $\mu^+$ ) are effective viscosities representing adhesive drag forces between normal (mutant) cells and the stroma. Combining the law of mass balance and Darcy's law, and writing  $p = \mu^- k^- \hat{p}$ ,  $\mathbf{v} = k^- \hat{\mathbf{v}}$  and  $t = \hat{t}/k^-$ , we have

$$\nabla^2 \hat{p} = -\mathcal{H}(H_W - y), \quad \text{outside } D, \quad (2.4)$$

where  $\mathcal{H}(H_W - y)$  is the Heaviside step function. For mutant cells,

$$\nabla^2 \hat{p} = -k \phi_M, \quad \text{inside } D, \quad (2.5)$$

where  $\phi_M = \mu^+/\mu^-$  represents the relative effective viscosity of mutant to normal cells and  $k = k^+/k^-$  is the relative proliferation rate. On  $\Gamma = 0$ , pressure and

normal velocity are continuous and  $\Gamma = 0$  moves as a material interface, such that

$$\phi_M \mathbf{n} \cdot \nabla \hat{p}|^- = \mathbf{n} \cdot \nabla \hat{p}|^+, \quad [\hat{p}]_+^0 = 0, \quad \frac{\partial \Gamma}{\partial \hat{t}} + \hat{\mathbf{v}} \cdot \nabla \Gamma = 0, \quad (2.6)$$

where  $\mathbf{n}$  is the unit normal to the interface and  $[.]_+^0$  is the difference in the values from each approach, + for mutant cells, – for normal cells. To close the model, no-flux conditions are imposed on the base and sides of the crypt,

$$\frac{\partial \hat{p}}{\partial y}(x, 0, t) = 0 \quad (2.7)$$

and

$$\frac{\partial \hat{p}}{\partial x}(0, y, t) = \frac{\partial \hat{p}}{\partial x}(W_C, y, t) = 0, \quad (2.8)$$

while to represent sloughing of cells from the top of the crypt we impose

$$\hat{p}(x, H_C, t) = 0. \quad (2.9)$$

We seek solutions symmetric about  $x = W_C/2$  using a collocation method, in which  $D$  represents a patch of mutant cells within the crypt (figure 2). A local polar coordinate system  $(r, \theta)$  centred on the mid-point of  $D$  is introduced and the solution of equations (2.5) and (2.8a) is represented as an expansion in  $r^m \cos(m\theta)$ ,  $m = 1, 2, \dots$ . Outside  $D$ , the solution of equations (2.4), (2.7), (2.8b) and (2.9) is represented as an expansion in  $\cos \omega_n y (\cos \omega_n w - \tanh(\omega_n H_C) \sinh(\omega_n x))$ , where  $\omega_n = (n - 1/2)\pi$ . Collocation points are distributed along  $x = W_C/2$  (outside  $D$ ) and  $\Gamma = 0$ . Enforcing the remaining boundary conditions yields a linear algebraic problem for the vector of coefficients in the expansions, solved by minimizing the residuals in the  $L_1$  norm. Representative results are shown in the electronic supplementary material.

### 3. Comparison of models

We use the above models to simulate a healthy crypt undergoing normal tissue renewal (crypt homeostasis), comparing the output from the cell-based and continuum models. We then investigate how the system dynamics change when a patch of mutant cells is introduced into the crypt.

#### (a) Crypt homeostasis

Typical simulation results for the cell-based models are presented in figure 3. Owing to the stochasticity inherent in the models, and since the components of the cell velocities satisfy  $v_y \gg v_x$ , average values of  $v_y$  were computed by splitting the crypt into horizontal bands of unit width, averaging  $v_y$  over all cells in a given band and repeating the process for 100 simulations; similar averages were obtained for the average area difference  $A_T - A$  and the number of vertices associated with each cell. The results are presented in figure 4 where they are compared with corresponding output from the continuum model. In each case, the velocity profile changes markedly between the proliferating ( $0 \leq y \leq H_W$ ) and non-proliferating ( $H_W \leq y \leq H_C$ ) regions. In the lower region,  $v_y$  increases linearly

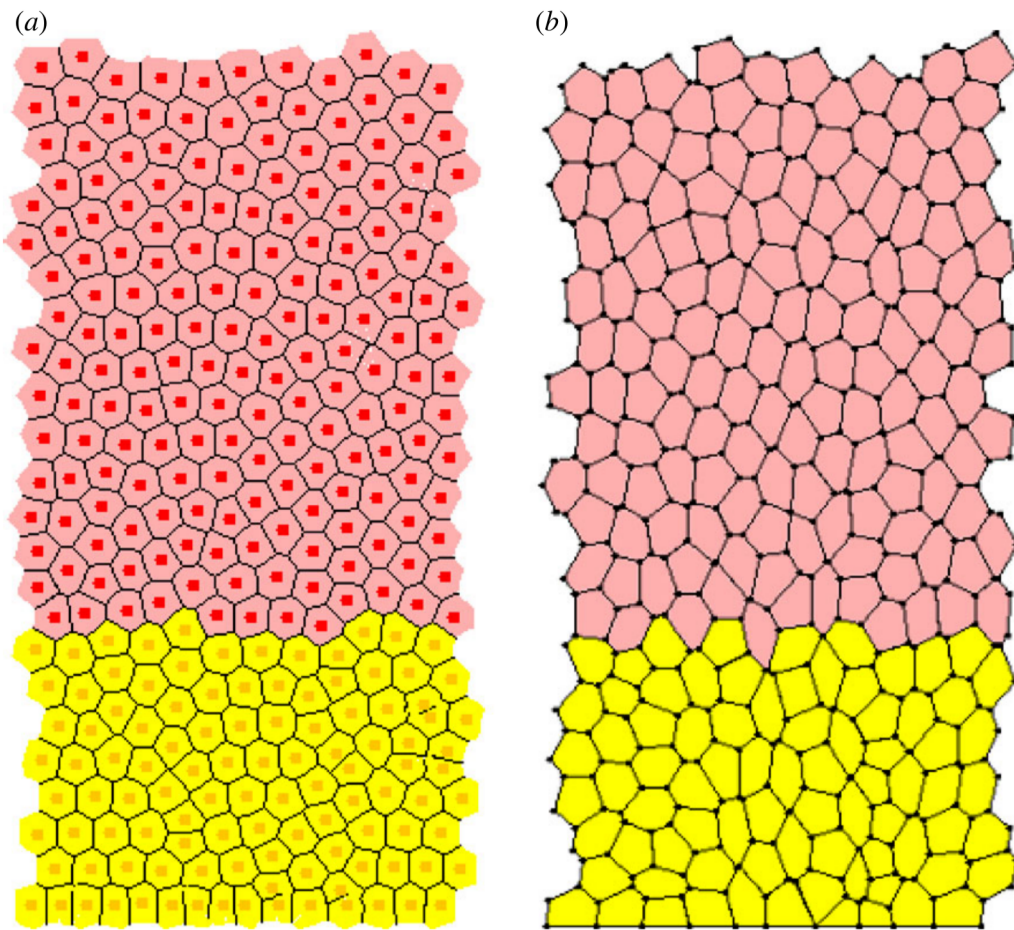


Figure 3. Example simulations using (a) the cell-centre model and (b) the cell-vertex model. Proliferating cells, yellow; non-proliferating cells, pink.

with distance from the crypt base for all three models (figure 4c). In the non-proliferating region, for the cell-based models,  $v_y$  still increases, albeit more slowly. This is because the non-proliferating cells relax and increase in size ( $(A_T - A)$  decreases; figure 4a), forcing those above them to move more quickly. Correspondingly, the pressure field in the continuum model falls from the base to the top of the crypt (figure 4b), indicating how cells would be compressed were such effects taken into account. However, in the continuum model, cell density is fixed, so  $v_y$  is uniform for  $y > H_W$  and the maximum cell velocity is higher than in the cell-based models (figure 4a). In the homeostatic state, proliferative expansion in the continuum model is entirely accommodated by vertical cell displacement, whereas in the cell-based models, it is accommodated to some extent by cell compression and some lateral displacement, leading to lower cell velocities.

Further inspection of our simulations reveals that cells near the crypt base are more compressed than those near the top (figure 4a,b), the decrease for the cell-based models being approximately linear in the non-proliferating zone. If we identify  $(A_T - A)$  with cell pressure, then figure 4a,c suggests that, in the non-proliferating region,  $v_y \propto d(A_T - A)/dx$ , which is consistent with Darcy's law (figure 4b). In the lower, proliferating region, the agreement between the cell-level and continuum models is poor because the cells in the continuum model are assumed to be incompressible. We note also that for both cell-based models

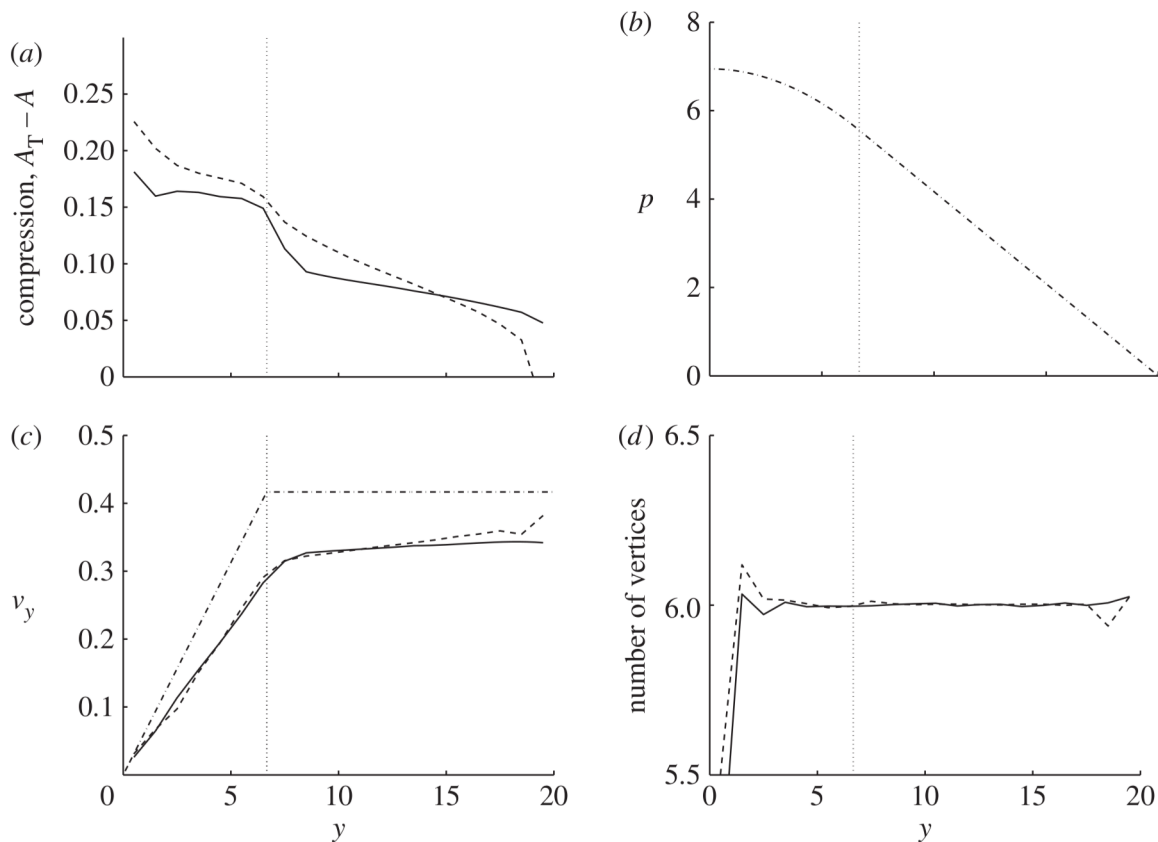


Figure 4. (a) Average area difference,  $A_T - A$ , varies with distance from the crypt base,  $y$ , for cell-centre and cell-vertex models. (b) The pressure,  $p$ , varies with  $y$  in the continuum model. (c) The averaged vertical component of the cell velocity,  $v_y$ , varies with  $y$  for all three models. (d) The average number of vertices for the cell-centre and cell-vertex models varies with  $y$ . Cell-vertex model, solid line; cell-centre model, dashed line; continuum model, dashed-dotted line. The dotted vertical line separates the Wnt-stimulated, proliferating region ( $0 < y \leq H_W$ ) from the non-proliferating one ( $y > H_W$ ).

the average number of cell vertices remains constant throughout the crypt at 6, apart from near the crypt base where the no-flux boundary conditions lead to cell distortion (figure 4d).

All three models reproduce the basic features of a healthy crypt: cells proliferate in the lower region, they migrate upwards and are sloughed off near the top. We now investigate how well the models reproduce other experimentally observed phenomena, such as crypt monoclonality.

There has been considerable debate about whether the cells within a crypt are polyclonal (emerging from multiple stem cells) or monoclonal. Recently, when Taylor *et al.* (2003) labelled mitochondrial DNA to track cell lineages, wave-like ribbons extending from the base to the top of the crypt were observed. The results presented in figure 5 show that the cell-based and continuum models yield similar qualitative behaviour (movies of these simulations are presented in the electronic supplementary material). While the cell-based models produce wavy lineages, the continuum model generates a vertical column since it predicts no azimuthal movement of cells in homeostasis. Consequently, the continuum model cannot be used to investigate whether crypts are monoclonal or polyclonal. By contrast, extending the duration of the cell-based simulations reveals that

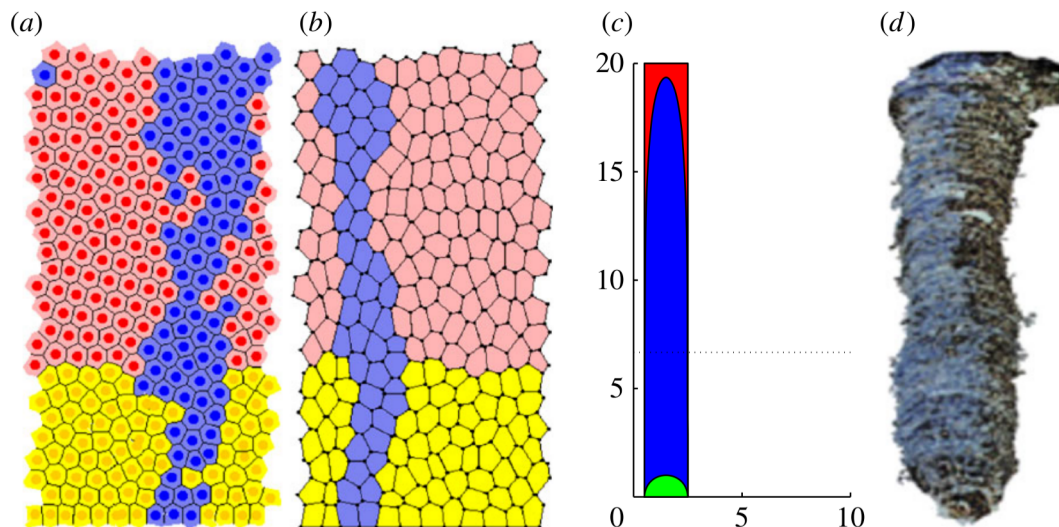


Figure 5. Snapshots of a cell lineage from: (a) the cell-centre model; (b) the cell-vertex model; (c) the continuum model; and (d) experiment (adapted from Taylor *et al.* 2003). Both cell-based models show marked cells moving as a wavy ribbon as in the experiments, and the continuum model predicts a uniform band of labelled cells. In (a,b), cells from the lineage are blue, transit cells are marked yellow and differentiated cells marked pink. In (c), the evolution of a labelled region of cells is tracked over time. Green,  $t = 0$ ; blue,  $t = 60$  and red,  $t = \infty$ . In (d), cells from the lineage are marked in blue, other cells are in black.

if cells at the base of the crypt move freely then it will eventually become monoclonal, whereas if they are fixed in position then the crypt will remain polyclonal (see figure 6 and van Leeuwen *et al.* 2009). These results, together with independent experimental confirmation that crypts are monoclonal (McDonald *et al.* 2006), lead us to predict that the (stem) cells at the base of a crypt move freely.

### (b) Crypt invasion by mutant cells

In this section, we study the ways in which a small patch of mutant cells can colonize a crypt during early CRC. Two hypotheses have been proposed to explain this phenomenon. Proponents of the ‘top-down’ theory argue that the first mutant cells appear near the top of the crypt and invade downwards into the crypt (Lamprecht & Lipkin 2002). Other authors argue that mutations originate in stem cells at the crypt base, migrate upwards and colonize the crypt via ‘bottom-up morphogenesis’ (Preston *et al.* 2003).

To compare the two hypotheses, we introduced, into a normal crypt, a circular patch of mutant cells, of radius 2 cell diameters, centred at  $(x, y) = (W_C/2, A_0)$ , and investigated how changes in the drag coefficient of the mutant cells and their initial vertical position,  $A_0$ , affected their ability to colonize the crypt. Recall that the drag force acts at the cell centre for the cell-centre model whereas in the cell-vertex model it is the average of the drag on the cells surrounding that vertex; in the continuum model the effects of cell–stroma adhesion are incorporated within the relative viscosity  $\phi_M$ . Simulation results from the cell-vertex and continuum models suggest that mutant cell invasion is predominantly ‘bottom-up’ but that ‘top-down’ invasion can occur if adhesive effects are strong (figure 7).

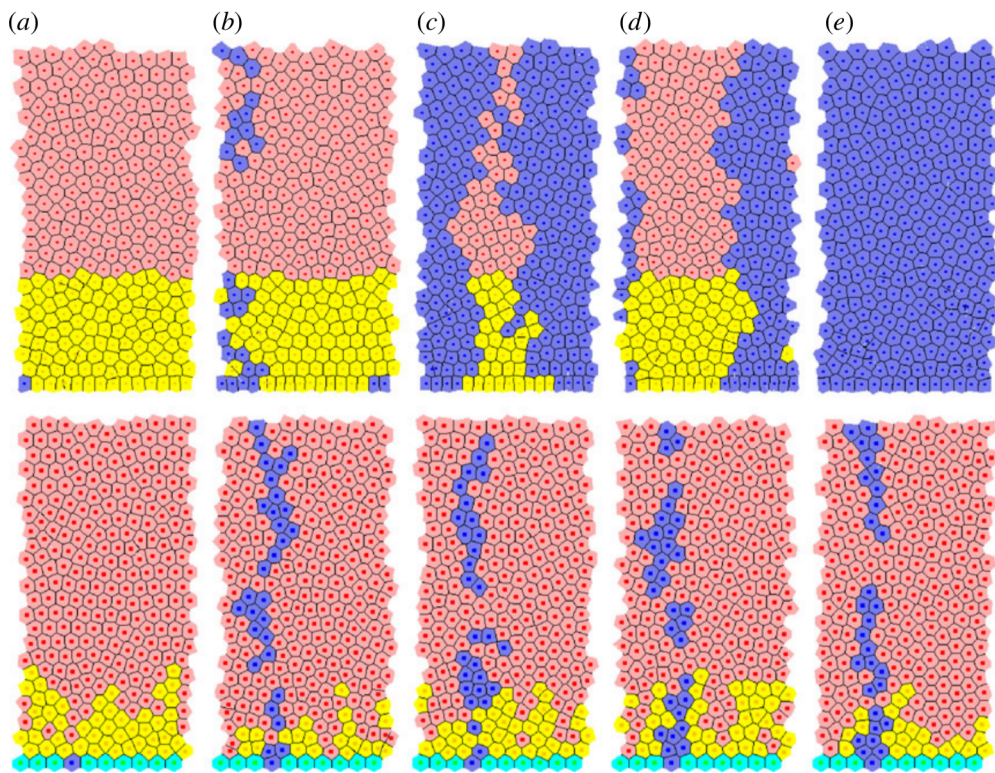


Figure 6. Results from two simulations of the cell-centre model showing how pinning the cells at the crypt base affects the distribution of cells within a normal crypt. In the lower plots, the cells at the crypt base are fixed in position and no single cell lineage dominates the crypt. When the cells at the crypt base are free to move (upper plots), the crypt eventually becomes monoclonal. The cell distributions are plotted at times  $t = 0, 250, \dots, 1000$  h for (a–e), respectively, and the colour code is the same as that used in figure 5a.

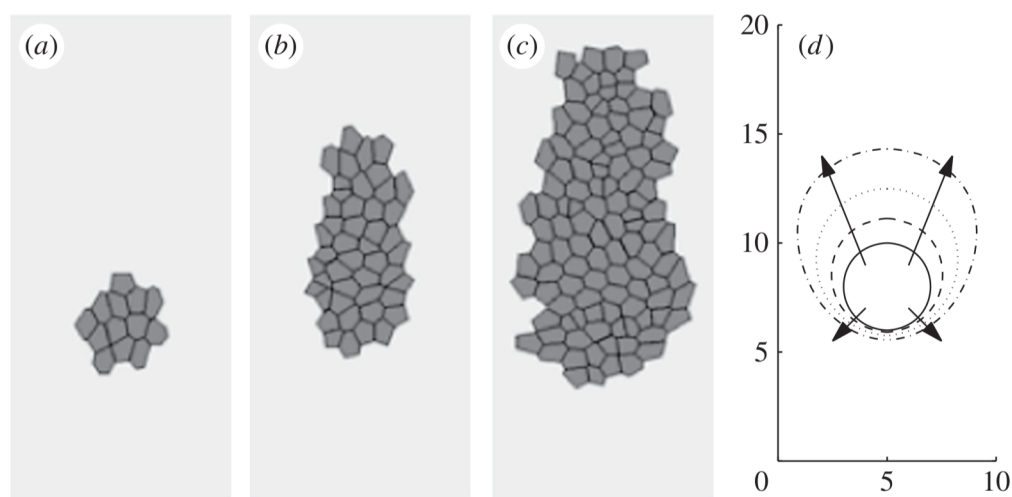


Figure 7. (a–c) Simulation results from the cell-vertex model showing how a patch of mutant cells initially moves up the crypt and then migrates down. The cell distributions in (a–c) correspond to times  $t = 0, 25$  and  $50$ , respectively. Parameter values are as in the electronic supplementary material, except  $\eta_M = 18\eta_N$ ,  $A_0 = 8$ . (d) Simulation results from the continuum model showing how a highly viscous patch of mutant cells ( $A_0 = 8$ ,  $B(0) = 6$ ,  $\phi_M = 15.0$ ,  $k = 1$ ) invades the crypt. The boundary separating the mutant and normal cells is plotted at times  $t = 0, 8, 16, 24$  h and the arrows indicate the direction of movement of the interface.

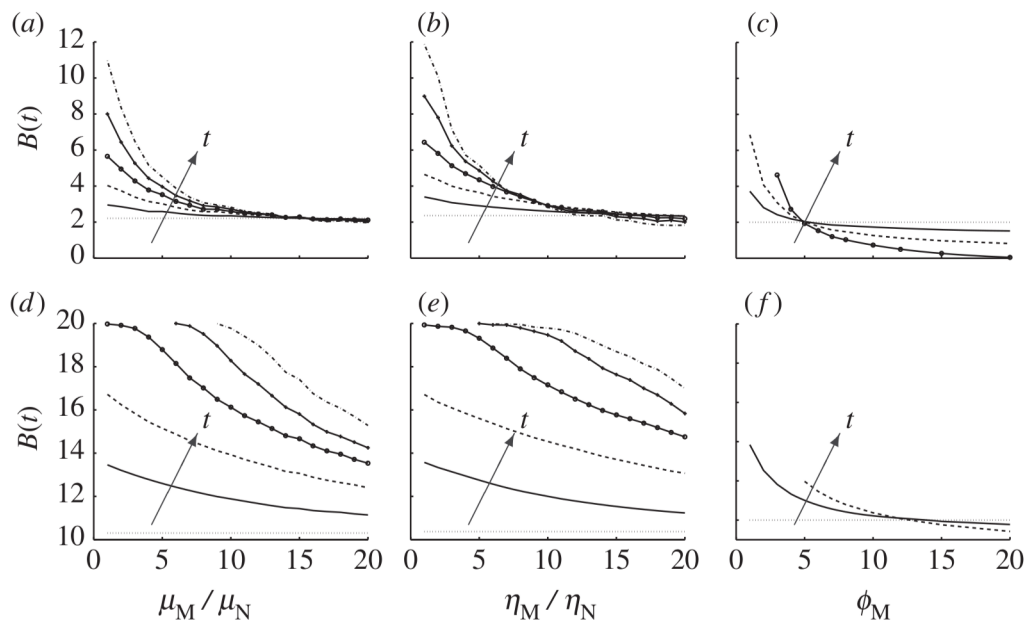


Figure 8. Plots showing how the vertical height of the centre of the lowest cell in the mutant patch,  $B(t)$ , changes over time as the initial vertical position of the mutant patch and the corresponding drag ratio vary. The initial patch is a circle of radius 2, centred at  $(x, y) = (W_C/2, A_0)$ . Results are plotted at times  $t = 0, 10, 20, 30, 40, 50$  h for (a,d) the cell-centre model, (b,e) the cell-vertex model and (c,f) the continuum model. (a–c)  $A_0 = 4$ ; (d–f)  $A_0 = 12$ .

In order to determine how the dynamics of the mutant patch are influenced by the way in which drag is modelled, the position,  $B(t)$ , of the lowest point of the patch was recorded every 10 h, with values averaged over 50 simulations for the cell-based models. The results presented in figure 8 show that the different models share many common features. For example, in all cases and for all values of  $A_0$ , as the drag coefficient of mutant cells increases, they move more slowly than the healthy cells and are more likely to persist in the crypt. This is because the mutant cells offer greater resistance to the proliferative force exerted on them by the normal cells beneath them (figure 8).

Another common feature is that the patch dynamics are influenced by its initial position and, in particular, the velocity of the normal cells near its base. For example, when  $A_0 = 4$  and  $B(0) \approx 2$ , mutant cells near the base of the crypt, where the velocity is low (figure 4c), are more likely to exhibit downward invasion than mutant cells near the base of crypts having  $A_0 = 12$  and  $B(0) \approx 10$  (figure 8). We remark also that the dynamics of patches with  $A_0 \geq 12$  and  $B(0) \gtrsim 10$  (figure 8d–f) are similar because the velocity of the normal cells near the top of the crypt does not vary markedly (figure 4c).

Some behaviour is model specific. For example, for certain parameter values (when  $\mu_M \gtrsim 14\mu_N$  in figure 8b), the mutant cells initially move up the crypt ( $B(t_1) > B(0)$ ,  $t_1 > 0$ ) but move down at later times ( $B(t_2) < B(t_1)$ ,  $t_2 > t_1$ ; figure 7). This phenomenon is peculiar to the cell-based models and arises because the mutant cells need time to establish a critical mass within the crypt. Thereafter, displacing the normal cells below the patch offers less resistance to the mutant cells than displacing the normal and mutant cells above it and downward invasion ensues. We note also that the cells in the continuum model have more azimuthal expansion than those in the cell-vertex model (figure 7).

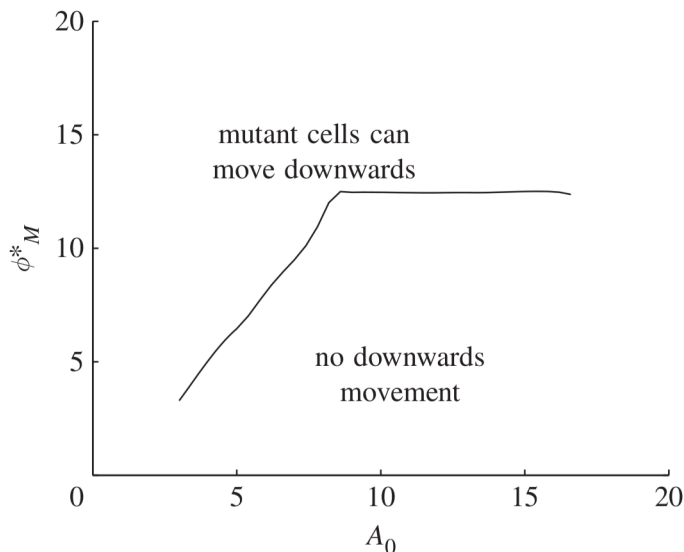


Figure 9. Bifurcation diagram showing how, for the continuum model, the minimum value of the relative viscosity needed for downward movement of cells at the base of the mutant patch,  $\phi_M^*$ , increases as the initial height of the centre of the mutant patch,  $A_0$ , increases. Parameter values:  $k = 1$ .

The cell-based results in figure 8 were obtained by averaging over 50 simulations. Given that the cell-centre and cell-vertex simulations take, respectively, 25 and 130 min to perform, it is clear that comprehensive parameter sensitivity analyses will be extremely time consuming. By contrast, such analyses are relatively straightforward with the continuum model. Indeed, figure 9 shows how, for the continuum model, the minimum value of the relative viscosity  $\phi_M$  needed to guarantee downward invasion of a patch of mutant cells increases as  $A_0$ , the initial height of the centre of the mutant patch, increases.

Experimental results indicate that Wnt-independent mutant cells have stronger cell–stroma adhesion than normal Wnt-dependent cells (Sansom *et al.* 2004). Our simulation results are consistent with these observations if we associate Wnt independence with increased drag. Our simulations also suggest that increased levels of adhesion (modelled by increased drag) are necessary for top-down morphogenesis. However, they also suggest that bottom-up morphogenesis is the dominant mechanism for invasion.

#### 4. Conclusions

In this paper, we have investigated the suitability of two cell-based models and a continuum model for simulating the cellular dynamics of intestinal crypts. We have shown that, while each model exhibits similar behaviour for many critical phenomena, there are model-specific differences. These findings suggest that more research must be carried out into the effects of using different individual cell-based models. This is a challenging research question because of the number of parameters involved and the fact that the way in which a biophysical process is incorporated may be model-dependent (consider, for example, the ways in which cell–cell adhesion is modelled in this paper). One possible approach may be to derive continuum descriptions from the discrete models. For example,

Murray *et al.* (2009) derived, from a simple one-dimensional spring-based model, a reaction–diffusion equation for cell density, while Lushnikov *et al.* (2008) used a statistical mechanics approach to derive a similar equation from a cellular Potts model. Crucially, both formulations contain a nonlinear diffusion coefficient that encapsulates the microscopic behaviour of the cells and depends on the assumptions made at this level. Comparison of the nonlinear diffusion coefficients reveals how macroscopic behaviour depends on model choice. The form of the resulting continuum model may also vary. For example, by considering the limit of large numbers of cells and assuming that cell parameters vary slowly, Fozard *et al.* (2009) derived a continuum description of a monolayer of tightly adherent, visco-elastic epithelial cells. The resulting model contains convective derivatives not normally associated with continuum tissue models.

Throughout the paper, we interpret ‘hybrid’ to mean a model in which cells are considered as discrete, and one of our justifications for considering cells as individuals is that for small cell numbers a continuum approach is not valid. As a tumour grows, the number of cells increases to an extent that a continuum description, at least in certain regions, is now valid. In such cases, ‘hybrid’ may refer to a model in which cells are viewed as discrete in some parts of the domain and as a continuum in others (e.g. Kim *et al.* 2007).

While we take the application area of our modelling approach to be cancer, it is important to note that most of the issues discussed arise in many areas of biology, including development, regenerative medicine and wound healing (e.g. Deutsch & Dormann 2005; Schnell *et al.* 2007).

The mechanical components of the cell-based models are purely deterministic. An interesting extension to the models would be to include stochasticity for the mechanical parameters. However, we anticipate that the effect on the results of the current study would be negligible.

There are many ways in which the idealized models of the colorectal crypt presented in this paper could be extended and modified. For example, we could model the cells as deformable, elastic spheres (Drasdo & Loeffler 2001) or we could use the cellular Potts model (Glazier & Graner 1993). Further work is needed to determine the level of detail needed to account for subcellular effects such as progress through the cell cycle, Wnt signalling, cross-talk between different signalling pathways and feedback between phenomena acting at different spatial scales. For example, while in van Leeuwen *et al.* (2009) a detailed model of the Wnt-signalling pathway (see van Leeuwen *et al.* 2007) was used to couple cell proliferation and cell–cell adhesion, it remains to be established how mechanical effects (e.g. cell compression) affect cell proliferation and how interactions between signalling pathways (e.g. Wnt and c-myc) are affected by mutations in one of the pathways (Barker *et al.* 2009).

We began this paper by posing the questions ‘which cell-based description should we use?’ and, ‘as cell numbers increase, how do we move from the discrete system to the continuum?’. By comparing two cell-based models with a continuum model of the intestinal crypt, we have shown that many of the experimentally observed features of the crypt are robust to changes in the modelling framework used. Establishing which model framework to use and what level of detail to include remain open questions. In the future, close collaboration between experimentalists and theoreticians and careful integration of data with mathematical models should help to resolve these issues.

The authors gratefully acknowledge financial support from the EPSRC awarded to A.W., A.G.F. and G.R.M. as part of the Integrative Biology programme (GR/572023/01) and to J.M.O as part of a Life Sciences Interface Doctoral Training Centre (DTC) studentship (EP/E501605/1). J.M.O. and A.G.F. are funded through the OCISB project (BB/D020190/1). S.K.K. is supported by a Systems Biology DTC studentship (EP/G50029/1). G.R.M. is supported by the European Commission PreDiCT project (DG-INFSO 224381). P.P. is supported by the EPSRC-funded OxMOS project (EP/D048400/1). P.K.M. was partially supported by a Royal Society Wolfson Research Merit Award. P.K.M. and H.M.B. acknowledge support from PMI2 (British Council).

## References

- Alarcón, T., Byrne, H. M. & Maini, P. K. 2003 A cellular automaton model for tumour growth in inhomogeneous environment. *J. Theor. Biol.* **225**, 257–274. (doi:10.1016/S0022-5193(03)00244-3)
- Barker, N. *et al.* 2009 Crypt stem cells as the cells-of-origin of intestinal cancer. *Nature* **457**, 608–611. (doi:10.1038/nature07602)
- Bienz, M. 2005  $\beta$ -catenin: a pivot between cell adhesion and Wnt signalling. *Curr. Biol.* **15**, 64–67. (doi:10.1016/j.cub.2004.12.058)
- Byrne, H. M., Owen, M. R., Alarcón, T., Murphy, J. & Maini, P. K. 2006 Modelling the response of vascular tumours to chemotherapy: a multiscale approach. *Math. Model. Methods Appl. Sci.* **16**, 1219–1241. (doi:10.1142/S0218202506001522)
- Deutsch, A. & Dormann, S. 2005 *Cellular automaton modeling of biological pattern formation: characterization, applications, and analysis*. Boston, MA: Birkhäuser.
- Drasdo, D. & Loeffler, M. 2001 Individual-based models to growth and folding in one-layered tissues: intestinal crypts and early development. *Nonlinear Anal.* **47**, 245–256. (doi:10.1016/S0362-546X(01)00173-0)
- Ferlay, J., Autier, P., Boniol, M., Heanue, M., Colombet, M. & Boyle, P. 2007 Estimates of the cancer incidence and mortality in Europe in 2006. *Ann. Oncol.* **18**, 581. (doi:10.1093/annonc/mdl498)
- Fozard, J. A., Jensen, O. E., Byrne, H. M. & King, J. R. 2009 Continuum approximations of individual-based models for multicellular systems. *Math. Med. Biol.* **27**, 39–74. (doi:10.1093/imammb/dqp015)
- Gaspar, C. & Fodde, R. 2004 APC dosage effects in tumorigenesis and stem cell differentiation. *Int. J. Dev. Biol.* **48**, 377–386. (doi:10.1387/ijdb.041807cg)
- Glazier, J. A. & Graner, F. 1993 Simulation of the differential adhesion driven rearrangement of biological cells. *Phys. Rev. E* **47**, 2128–2154. (doi:10.1103/PhysRevE.47.2128)
- Greenspan, H. P. 1976 On the growth and stability of cell cultures and solid tumors. *J. Theor. Biol.* **56**, 2. (doi:10.1016/S0022-5193(76)80054-9)
- Honda, H., Yamanaka, H. & Dan-Sohkawa, M. 1984 A computer simulation of geometrical configurations during cell division. *J. Theor. Biol.* **106**, 423–435. (doi:10.1016/0022-5193(84)90039-0)
- Jemal, A., Siegel, R., Ward, E., Hao, Y., Xu, J. & Thun, M. J. 2009 Cancer statistics, 2009. *CA: Cancer J. Clin.* **59**, 225. (doi:10.3322/caac.20006)
- Kim, Y., Stolarska, M. A. & Othmer, H. G. 2007 A hybrid model for tumor spheroid growth in vitro I: theoretical development and early results. *Math. Model. Methods Appl. Sci.* **17**, 1773. (doi:10.1142/S0218202507002479)
- Lamprecht, S. A. & Lipkin, M. 2002 Migrating colonic crypt epithelial cells: primary targets for transformation. *Carcinogenesis* **23**, 1777–1780. (doi:10.1093/carcin/23.11.1777)
- Lushnikov, P. M., Chen, N. & Alber, M. 2008 Macroscopic dynamics of biological cells interacting via chemotaxis and direct contact. *Phys. Rev. E* **78**, 61904. (doi:10.1103/PhysRevE.78.061904)
- Martins, M. L., Ferreira, S. C. & Vilela, M. J. 2007 Multiscale models for the growth of avascular tumors. *Phys. Life Rev.* **4**, 128–156. (doi:10.1016/j.plrev.2007.04.002)

- McDonald, S. A., Preston, S. L., Greaves, L. C., Leedham, S. J., Lovell, M. A., Jankowski, J. A., Turnbull, D. M. & Wright, N. A. 2006 Clonal expansion in the human gut: mitochondrial DNA mutations show us the way. *Cell Cycle* **5**, 808–811.
- McDougall, S. R., Anderson, A. R. A., Chaplain, M. A. J. & Sherratt, J. A. 2002 Mathematical modelling of flow through vascular networks: implications for tumour-induced angiogenesis and chemotherapy strategies. *Bull. Math. Biol.* **64**, 673–702. (doi:10.1006/bulm.2002.0293)
- Meineke, F. A., Potten, C. S. & Loeffler, M. 2001 Cell migration and organization in the intestinal crypt using a lattice-free model. *Cell Prolif.* **34**, 253–266. (doi:10.1046/j.0960-7722.2001.00216.x)
- Merks, R. M. H. & Glazier, J. A. 2005 A cell-centered approach to developmental biology. *Physica A* **352**, 113–130. (doi:10.1016/j.physa.2004.12.028)
- Murray, P. J., Edwards, C. M., Tindall, M. J. & Maini, P. K. 2009 From a discrete to a continuum model of cell dynamics in one dimension. *Phys. Rev. E* **80**, 031912. (doi:10.1103/PhysRevE.80.031912)
- Nagai, T. & Honda, H. 2001 A dynamic cell model for the formation of epithelial tissues. *Phil. Mag. B* **81**, 699–719. (doi:10.1080/13642810108205772)
- Owen, M. R., Alarcón, T., Maini, P. K. & Byrne, H. M. 2009 Angiogenesis and vascular remodelling in normal and cancerous tissues. *J. Math. Biol.* **58**, 689–722. (doi:10.1007/s00285-008-0213-z)
- Patel, A. A., Gawlinsky, E. T., Lemieux, S. K. & Gatenby, R. A. 2001 Cellular automaton model of early tumour growth and invasion: the effects of native tissue vascularity and increased anaerobic tumour metabolism. *J. Theor. Biol.* **213**, 315–331. (doi:10.1006/jtbi.2001.2385)
- Pitt-Francis, J. *et al.* 2009 Chaste: a test-driven approach to software development for biological modelling. *Comput. Phys. Commun.* **180**, 2452–2471. (doi:10.1016/j.cpc.2009.07.019)
- Preston, S. L. *et al.* 2003 Bottom-up histogenesis of colorectal adenomas: origin in the monocryptal adenoma and initial expansion by crypt fission. *Cancer Res.* **63**, 3819–3825.
- Preziosi, L. & Tosin, A. 2009 Multiphase and multiscale trends in cancer modelling. *Math. Model. Nat. Phenom.* **4**, 1–11. (doi:10.1051/mmnp/20094301)
- Sansom, O. J. *et al.* 2004 Loss of Apc *in vivo* immediately perturbs Wnt signalling, differentiation, and migration. *Genes Dev.* **18**, 1385–1390. (doi:10.1101/gad.287404)
- Sausedo, R. A., Smith, J. L. & Schoenwolf, G. C. 1997 Role of nonrandomly oriented cell division in shaping and bending of the neural plate. *J. Compar. Neurol.* **381**, 473–488.
- Schnell, S., Grima, R. & Maini, P. K. 2007 Multiscale modeling in biology. *Am. Scient.* **95**, 134–142.
- Shirinifard, A., Gens, J. S., Zaitlen, B. L., Poplawski, N. J., Swat, M. & Glazier, J. A. 2009 3D multi-cell simulation of tumor growth and angiogenesis. *PLoS ONE* **4**, e7190. (doi:10.1371/journal.pone.0007190)
- Smallbone, K., Gatenby, R. A., Gillies, R. J., Maini, P. K. & Gavaghan, D. J. 2007 Metabolic changes during carcinogenesis: potential impact on invasiveness. *J. Theor. Biol.* **244**, 703–713. (doi:10.1016/j.jtbi.2006.09.010)
- Sunter, J. P., Appleton, D. R., Dé Rodriguez, M. S., Wright, N. A. & Watson, A. J. 1979 A comparison of cell proliferation at different sites within the large bowel of the mouse. *J. Anat.* **129**, 833–842.
- Taylor, R. W. *et al.* 2003 Mitochondrial DNA mutations in human colonic crypt stem cells. *J. Clin. Invest.* **112**, 1351–1360.
- van Leeuwen, I. M. M., Byrne, H. M., Jensen, O. E. & King, J. R. 2007 Elucidating the interactions between the adhesive and transcriptional functions of β-catenin in normal and cancerous cells. *J. Theor. Biol.* **247**, 77–102. (doi:10.1016/j.jtbi.2007.01.019)
- van Leeuwen, I. M. M. *et al.* 2009 An integrative computational model for intestinal tissue renewal. *Cell Prolif.* **42**, 617–636. (doi:10.1111/j.1365-2184.2009.00627.x)
- Zheng, X., Wise, S. M. & Cristini, V. 2005 Nonlinear simulation of tumor necrosis, neovascularization and tissue invasion via an adaptive finite-element/level-set method. *Bull. Math. Biol.* **67**, 211–259. (doi:10.1016/j.bulm.2004.08.001)